Time Domain Description of Optical MIMO Channels

André Sandmann[1], Andreas Ahrens[2], Steffen Lochmann[3]

Hochschule Wismar, University of Technology, Business and Design,
Philipp-Müller-Straße 14, 23966 Wismar, Germany
[1]a.sandmann@stud.hs-wismar.de, [2]andreas.ahrens@hs-wismar.de,
[3]steffen.lochmann@hs-wismar.de

Abstract

Within the last years Multiple-Input Multiple-Output (MIMO) transmission has reached a lot of attention in the optical fibre community. Theoretically, the concept of MIMO is well understood. However, practical implementations of optical components are in the focus of interest for further computer simulations. That's why in this contribution the specific impulse responses of the (2×2) MIMO channel, including a 1.4 km multi-mode fibre and optical couplers at both ends, are measured for operating wavelengths of 1326 nm and 1576 nm. Since semiconductor diode lasers, capable of working at different wavelengths, are used for the characterization of the underlying optical MIMO channel, inverse filtering is needed for obtaining the respective impulse responses. However, the process of inverse filtering also known as signal deconvolution is critical in noisy environments. That's why different approaches such as Wiener and parametric filtering are studied with respect to different optimization criteria. Moreover, different measurement impacts on the impulse response, such as offset compensation, timing and synchronisation etc., will be investigated. Using these obtained impulse responses a baseband MIMO data transmission is modelled. In order to create orthogonal channels enabling a successful transmission, a MIMO zero–forcing (ZF) equaliser is implemented and analysed. Our main results given as an open eye-diagram and calculated bit-error rates show the successful implementation of the MIMO transmission system.

1 Introduction

Aiming at further increasing the fibre capacity in optical transmission systems the concept of MIMO, well studied and wide-spread in radio transmission systems, has led to increased research activities in this area [1–3]. Theoretical investigations have shown that similar capacity increases are possible compared to wireless systems [4, 5]. The basis for this approach is the exploitation of the different optical mode groups.

However, the practical implementation has to cope with many technological obstacles such as mode multiplexing and management. This includes mode combining, mode maintenance and mode splitting. In order to improve existing simulation tools practical measurements are needed. That's why in this contribution a whole optical transmission testbed is characterized by its respective impulse responses obtained by high-bandwidth measurements.

In order to describe the optical MIMO testbed at different operating wavelengths semiconductor laser diodes with a pulse width of 25 ps are used. Since the used picosecond laser generator doesn't guarantee a fully flat frequency spectrum in the region of interest, inverse filtering has to be applied to obtain the MIMO impulse responses. However, the process of inverse filtering also known as signal deconvolution is critical in noisy environments. That's why different approaches such as Wiener and parametric filtering are studied with respect to different optimization criteria such as the mean square error (MSE) and the imaginary error parameter introduced by Gans [6].

Using the measured impulse responses a MIMO baseband transmission system can be constructed. In order to exploit the full potential of the MIMO system, properly selected signal processing strategies have to be applied. The focus of this work is on the whole testbed functionality including the signal processing needed to separate the data streams. Based on computer simulations the end-to-end functionality of the whole testbed is demonstrated and appropriate quality criteria such as the eye-diagram and the the bit-error rate (BER) are calculated.

The novelty of this paper is given by the proven testbed functionality, which includes the whole electro-optical path with the essential optical MIMO components of mode combining and splitting. The next logical step is the implementation of the MIMO receiver modules such as automatic clock recovery, frame synchronisation, channel estimation and equalisation as demonstrated in [7].

The remaining part of the paper is structured as follows: In Section 2 the optical MIMO testbed and its corresponding system model are introduced. The further processing of the measured impulse responses, which is carried out by inverse filtering, is described in Section 3. The obtained results are given in Section 4. Finally, Section 5 shows our concluding remarks.

2 Optical MIMO System Model

An optical MIMO system can be formed by feeding different sources of light into the fibre, which activate different optical mode groups. This can be carried out by using centric and eccentric light launching conditions and subsequent combining of the activated different mode groups with a fusion coupler as show in Fig. 1 [8,9]. The different sources of light lead to different power distribution patterns at the fibre end depending on the transmitter side light launch conditions. Fig. 2 highlights the measured mean power distribution pattern at the end of a 1.4 km multi-mode fibre. At the end of the MMF transmission line a

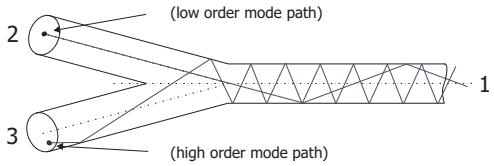

Figure 1: Transmitter side fusion coupler for launching different sources of light into the MMF

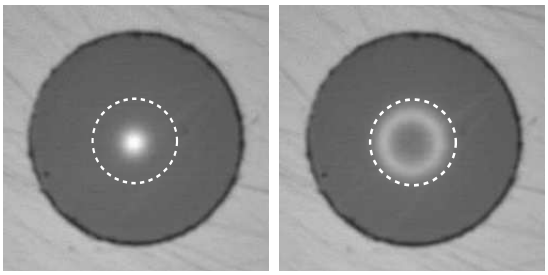

Figure 2: Measured mean power distribution pattern when using the fusion coupler at the transmitter side (left: centric mode excitation; right: eccentric mode excitation); the dotted line represents the 50 μm core size.

similar fusion coupler is used for splitting the different mode groups. The measurement setup depicted in Fig. 3 shows the testbed with the utilized devices for measuring the system properties of the optical MIMO channel in form of its specific impulse responses needed for modelling the MIMO data transmission. A picosecond laser unit is chosen for generating the 25 ps input pulse. This input pulse is used to measure separately the different Single-Input Single-Output (SISO) channels within the MIMO system. Since the used picosecond laser unit doesn't guarantee a fully flat frequency spectrum in the region of interest, the captured signals have to be deconvolved. The obtained impulse responses are forming the base for modelling the MIMO transmission system. Fig. 4 highlights the resulting electrical MIMO system model.

3 Measurement Campaign and Signal Deconvolution

Since the process of signal deconvolution is critical in noisy environments, different filtering processes such as Wiener and parametric filtering are studied in order to guarantee a high quality of the deconvolution process defined by the mean square error (MSE) and the imaginary error parameter introduced by Gans [6].

A linear time-invariant system is defined uniquely by its impulse response, or its Fourier transform as the corresponding transfer function. For the determination of the impulse response $g_{\mathrm{k}}(t)$ (see also Fig. 5) an appropriate formed input signal $u_1(t)$ is needed. Unfortunately, an ideal Dirac delta pulse with a frequency independent transfer function is practically not viable. In real systems adequate impulses compared to the Dirac delta pulse must be used. For the determination of the impulse response in optical transmission systems impulses as specified in [10] have proven to be useful. Additionally, when

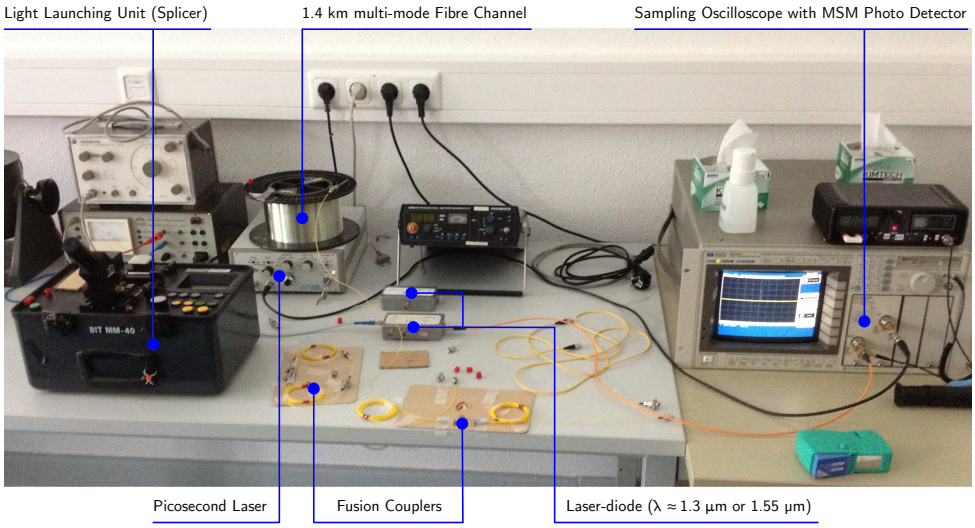

Figure 3: Measurement setup for determining the MIMO specific impulse responses.

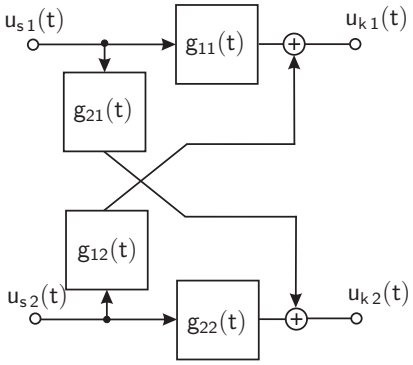

Figure 4: Electrical MIMO system model (example: $n = 2$)

analysing the characteristics of any practical system, the measured impulse $u_3(t)$ is affected by noise. The resulting transmission system model is depicted in Fig. 5. The

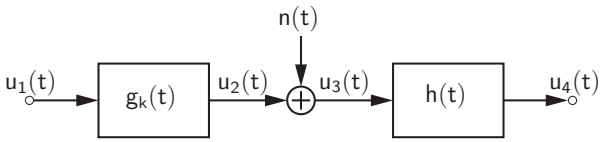

Figure 5: Transmission system model.

measured impulse $u_3(t)$ can be decomposed into two parts, namely, the low-pass filtered output signal $u_2(t)$ and the noise part $n(t)$ resulting in

$$u_3(t) = u_1(t) * g_\mathrm{k}(t) + n(t) \quad . \tag{1}$$

In the absence of the noise term, i. e. $n(t) = 0$, the system characteristic $g_\mathrm{k}(t)$ can be easily obtained by inverse filtering and is given as

$$g_\mathrm{k}(t) \quad \circ\!\!-\!\!\bullet \quad G_\mathrm{k}(f) = \frac{U_3(f)}{U_1(f)} \quad . \tag{2}$$

Unfortunately, the measured impulse $u_3(t)$ is affected by the noise term $n(t)$. Under these conditions inverse filtering is not working properly anymore. In order to improve the quality of the signal deconvolution different filter functions $h(t)$ are applied and the filtered signal results in

$$u_4(t) = u_1(t) * g_\mathrm{k}(t) * h(t) + n(t) * h(t) \ . \tag{3}$$

This filter operation affects both the low-pass filtered output signal $u_2(t)$ and the noise term $n(t)$. With an appropriate selected filter function the estimation of the impulse response $g_\mathrm{k}(t)$ yields to

$$\hat{g}_\mathrm{k}(t) \quad \circ\!\!-\!\!\bullet \quad \hat{G}_\mathrm{k}(f) = \frac{U_4(f)}{U_1(f)} \ . \tag{4}$$

Hereinafter, two different filter functions types are studied to estimate the impulse response $g_\mathrm{k}(t)$ based on the measured impulse $u_3(t)$. Commonly, the mean square error (MSE) between the impulse response $g_\mathrm{k}(t)$ and the estimated impulse response $\hat{g}_\mathrm{k}(t)$ is chosen as a quality indicator. It is expressed as

$$F_\mathrm{MSE} = \mathrm{E}\{[g_\mathrm{k}(t) - \hat{g}_\mathrm{k}(t)]^2\} \quad \longrightarrow \quad \text{min.} \ , \tag{5}$$

where $\mathrm{E}\{\cdot\}$ denotes the expectation functional.

Firstly, the Wiener filter $h_\mathrm{w}(t)$ is investigated. It is based on finding the optimal solution for minimizing the MSE when comparing the signal $u_2(t)$ with the filter output signal $u_4(t)$. It is calculated as

$$\mathrm{E}\{[u_2(t) - u_3(t) * h_\mathrm{w}(t)]^2\} \quad \longrightarrow \quad \text{min.} \ , \tag{6}$$

Assuming the signal $u_2(t)$ and the noise $n(t)$ are uncorrelated, the Wiener filter transfer function results in [11, pp. 191-194]

$$H_\mathrm{w}(f) = \frac{S_{22}(f)}{S_{22}(f) + S_\mathrm{nn}(f)} \ , \tag{7}$$

where $S_{22}(f)$ is the power spectral density (PSD) of the signal $u_2(t)$ and $S_\mathrm{nn}(f)$ is the noise PSD of the signal $n(t)$.

A more simple filter choice when estimating the impulse response $g_\mathrm{k}(t)$ is represented by predefined parametric filter functions. Two one-parametric filters with the transfer function structure

$$H(f) = \frac{|U_1(f)|^2}{|U_1(f)|^2 + \gamma \cdot |X(f)|^2} \ , \qquad \gamma \in \mathbb{R} \tag{8}$$

are analysed. The regularisation filter presented in [12] and studied more closely in [13] is given by

$$H_\mathrm{R}(f) = H(f) \quad \text{with } X(f) = C(f) \ , \tag{9}$$

where:

$$|C(f)|^2 = 6 - 8\cos(2\pi f T_\mathrm{a}) + 2\cos(4\pi f T_\mathrm{a}) \tag{10}$$

and T_a is the sampling period. The second one-parametric filter described by Nahman and Guillaume is of the same structure and expressed as follows

$$H_\mathrm{N}(f) = H(f) \quad \text{with } X(f) = D(f) \ , \tag{11}$$

where:

$$|D(f)|^2 = (2\,\pi\,T_\mathrm{a}\,f)^4 \ . \tag{12}$$

The regularisation filter $H_\mathrm{R}(f)$ and the Nahman-Guillaume filter $H_\mathrm{N}(f)$ are low-pass filters with the parameter γ influencing the sharpness of the filters and hence determining the cutoff frequencies. The amplitude density spectrum $U_1(f)$ and the γ parameter have the unit Vs. Hereinafter, the unit of γ is not mentioned explicitly. Fig. 6 shows that the transfer function of both filters look consimilar. In order to appropriately select the

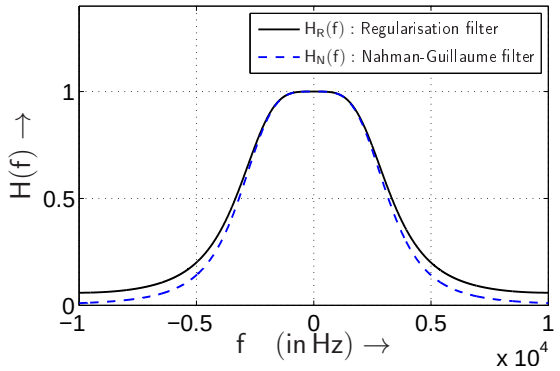

Figure 6: Comparison between the Regularisation filter $H_\mathrm{R}(f)$ and the Nahman-Guillaume filter $H_\mathrm{N}(f)$ with the parameters $U_1(f) = 1$ Vs, $\gamma = 1$ and $T_\mathrm{a} = 50\,\mu$s.

γ-parameter the MSE criterion (5) can be applied for the optimisation. In practical measurements the knowledge of the original impulse response $g_\mathrm{k}(t)$ is not given. Therefore, another criterion is needed in order to properly select the γ-parameter for practical measurements. A promising criterion was introduced by Gans [6], where the root mean square of the deconvolved imaginary part of $\hat{g}_\mathrm{k}(t)$ is used for finding the parameter of the regularisation function. This optimisation criterion can be expressed as

$$F_\mathrm{Gans} = \mathrm{E}\{[\mathrm{Im}\{\hat{g}_\mathrm{k}(t,\gamma)\}]^2\} \quad \longrightarrow \quad \text{min.} \ . \tag{13}$$

Using this criterion multiple local minima can occur and therefore another criterion described by Nahman and Guillaume in [12, pp. 22] should be taken into consideration when choosing the γ value of the regularisation filter. This error criterion is defined as the MSE between the measured receive signal $u_3(t)$ and the simulated receive signal $u_1(t) * \hat{g}_\mathrm{k}(t,\gamma)$,

filter	filter equation	used optimization criterion	signal knowledge necessary	practically applicable
Wiener filter	(7)	$\mathrm{E}\{[u_2(t) - u_3(t) * h_\mathrm{w}(t)]^2\}$	$u_3(t)$, $u_1(t)$, $u_2(t)$	×
$H_\mathrm{R}(f)$ & $H_\mathrm{N}(f)$	(9), (11)	$F_\mathrm{MSE} = \mathrm{E}\{[g_\mathrm{k}(t) - \hat{g}_\mathrm{k}(t)]^2\}$	$u_3(t)$, $u_1(t)$, $g_\mathrm{k}(t)$	×
$H_\mathrm{R}(f)$ & $H_\mathrm{N}(f)$	(9), (11)	$F_\mathrm{Gans} = \mathrm{E}\{[\mathrm{Im}\{\hat{g}_\mathrm{k}(t,\gamma)\}]^2\}$	$u_3(t)$, $u_1(t)$	✓

Table 1: filters and optimisation criteria at a glance

where $u_1(t)$ is the measured input impulse. It is described as follows

$$F_\mathrm{Error}(\gamma) = \mathrm{E}\{[u_3(t) - u_1(t) * \hat{g}_\mathrm{k}(t,\gamma)]^2\} \ . \tag{14}$$

Table 1 gives an overview of all filters and criteria.

In order to compare the quality of the estimated impulse responses using the one-parametric filters to the quality achieved by the Wiener filter, the following system is studied: The input impulse is a Dirac delta pulse with $u_1(t) = U_\mathrm{s}\, T_\mathrm{s}\, \delta(t)$, with $U_s = 1$ V, $T_\mathrm{s} = 1$ ms and $T_\mathrm{s}/T_\mathrm{a} = 20$. The chosen impulse response is

$$g_\mathrm{k}(t) = \frac{1}{T_\mathrm{s}} \ \mathrm{rect}\left(\frac{t}{T_\mathrm{s}}\right) \ . \tag{15}$$

In this case the filter output signal $u_2(t)$ is an rectangular impulse with the amplitude U_s. The deconvolution quality results are depicted in Fig. 7 as a function of the signal-to-noise-ratio E_s/N_0 with the parameter E_s defining the signal energy of $u_2(t)$ and the noise power spectral density N_0 of the signal $n(t)$. When applying the one-parametric

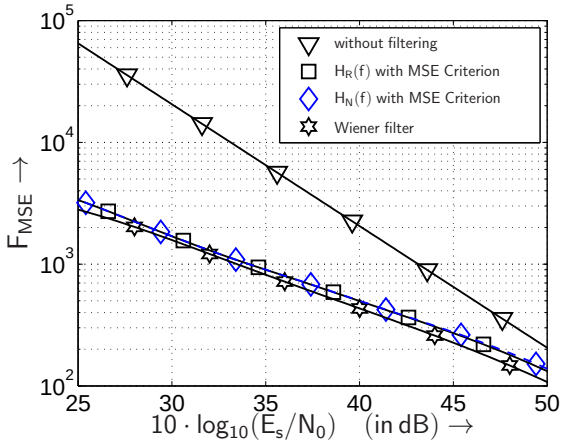

Figure 7: Quality F_MSE of the deconvolved impulse responses as a function of signal energy to noise power spectral density using different filter functions.

filters $H_\mathrm{R}(f)$ and $H_\mathrm{N}(f)$ the optimal γ values as well as the MSE are decreasing with increasing E_s/N_0. The achievable quality of the estimated impulse responses using the one-parametric filters together with the MSE optimisation criterion is nearly identical and comes close to the Wiener filter results. The benefit of using a filter function is clearly visible.

In order to determine the quality of the estimated impulse responses, which are practically obtainable using the Gans' criterion (13), the following optical system configuration

is studied: The measured input impulse of the picosecond laser is depicted in Fig. 8 for different operating wavelengths with a pulse width of approximately 25 ps. For the following simulation the operating wavelength is chosen to be 1576 nm. The impulse response

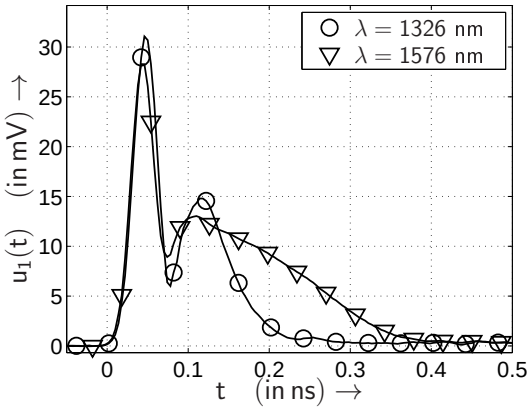

Figure 8: Measured input impulses at different operating wavelengths λ.

is carried out as a first-order low pass filter and is described as follows

$$G_{\mathrm{k}}(f) = A \cdot \frac{1}{1 + \mathrm{j}\, 2\,\pi\, f\, T_1} \quad , \tag{16}$$

where $T_1 = T_{\mathrm{s}} = 0.8$ ns and $T_{\mathrm{s}}/T_{\mathrm{a}} = 200$. The scaling factor A is chosen to maintain $E_s/T_s = 1\,\mathrm{V}^2$ of the signal $u_2(t)$ and to ensure the unit s^{-1} of the impulse response. Fig. 9 shows the quality of the obtained impulse responses using the filter functions mentioned before. The regularisation filter and the Nahman-Guillaume filter are applied for both optimisation criteria resulting in γ values depicted in Fig. 9. The γ values are also

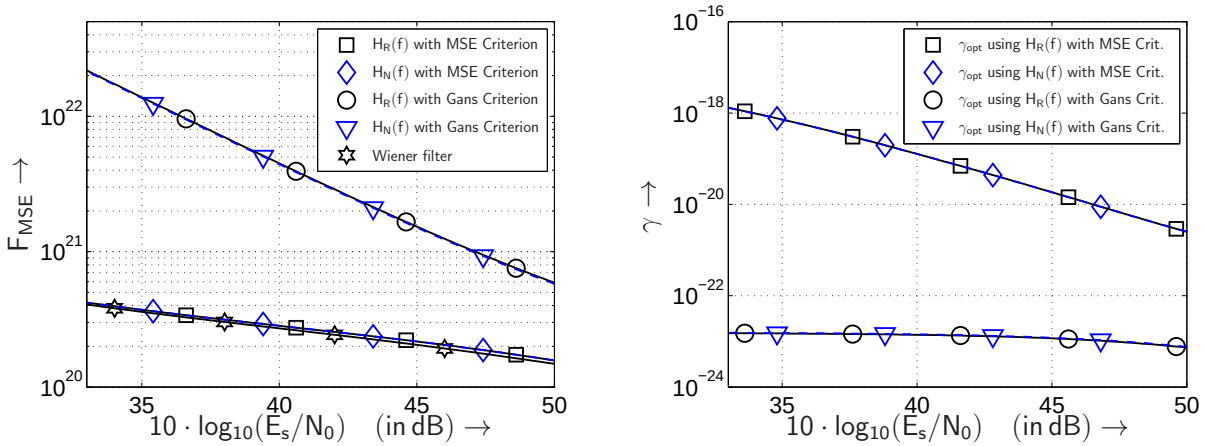

Figure 9: left: Quality F_{MSE} of the deconvolved impulse responses as a function of signal energy to noise power spectral density using different filters. right: Choice of optimal γ when filtering with the regularisation filter $H_{\mathrm{R}}(f)$ and the Nahman-Guillaume filter $H_{\mathrm{N}}(f)$ minimizing the MSE and using the Gans' criterion.

decreasing with increasing E_{s}/N_0 for both criteria. It should be noted, that the γ values using the Gans' criterion are lower compared to the MSE criterion. This signifies that

the measured signal $u_3(t)$ is filtered less when applying the filter using the Gans' criterion in contrast to using the MSE criterion. As expected, the deconvolved impulse responses using the Wiener filter are showing the best quality of all applied filter functions closely followed by the estimated impulse responses filtered with the one-parametric filters using the MSE optimisation criterion. The quality of the estimated impulse responses using the Gans' criterion is still acceptable for a wide range of E_s/N_0 values and is a major improvement comparing to the quality without filtering (not depicted). The obtained results show further that both parametric filters, whose quality is nearly identical, are a good compromise compared to the Wiener filter with its high complexity.

Applying the described deconvolution processing to the (2×2) MIMO testbed, the obtained impulse responses are depicted in Fig. 10. They are calculated by applying the regularisation filter in the deconvolution process with γ values respecting the Gans' and Error criterion. At an operating wavelength of 1326 nm the modal structure can

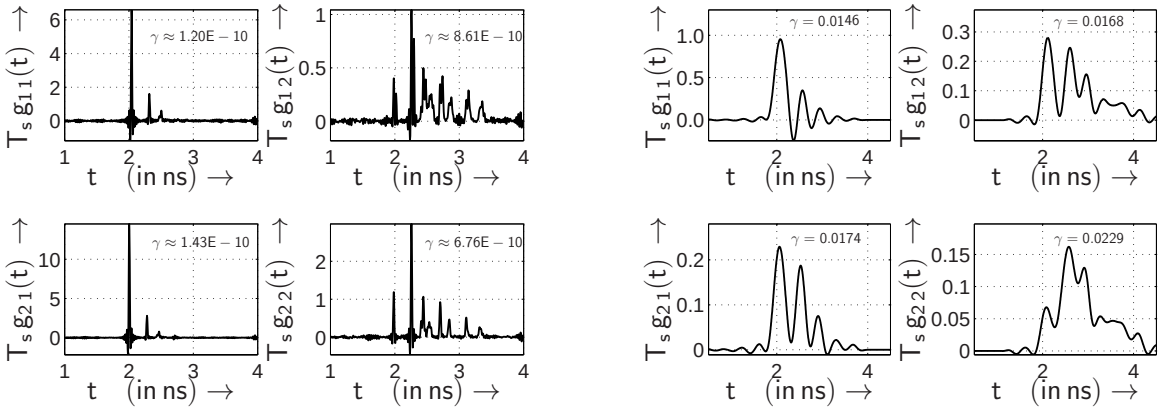

Figure 10: Deconvolved measured electrical MIMO impulse responses with respect to the pulse frequency $f_T = 1/T_s = 620$ MHz at 1326 nm (left) and 1576 nm operating wavelength (right) using the regularisation filter function with γ values according to the Gans' criterion.

be identified. Considering the 1576 nm results the additional influence of the chromatic dispersion is clearly visible.

4 MIMO Equalisation and Simulation Results

In this section the MIMO baseband transmission system is constructed as illustrated in Fig. 11. It uses the deconvolved (2×2) MIMO specific impulse responses $g_{i,j}(t)$ (for $i = 1, 2$ and for $j = 1, 2$) depicted in Fig. 10 at 1576 nm operating wavelength. In this baseband system model the transmitter forms a rectangular pulse train and hence the transmit filter $g_s(t)$ and the receive filter $g_{ef}(t)$ are considered to be matched filters and are described in its non causal notation with

$$g_s(t) = g_{ef}(t) = \frac{1}{T_s} \operatorname{rect}\left(\frac{t}{T_s}\right) \quad . \tag{17}$$

The total transmit power is normalised to $P_\mathrm{s} = 1\,\mathrm{V}^2$ and a symbol pulse frequency of $f_\mathrm{T} = 1/T_\mathrm{s} = 620$ MHz per data channel is used resulting in a total bit rate of 1.24 Gb/s for both channels. Both transmit signals $u_{\mathrm{s},j}(t)$ are launched onto the (2×2) MIMO channel. The filtered receive signals $u_{\mathrm{e},i}(t)$ are sampled with kT_s, where $k \in \mathbb{Z}$. The

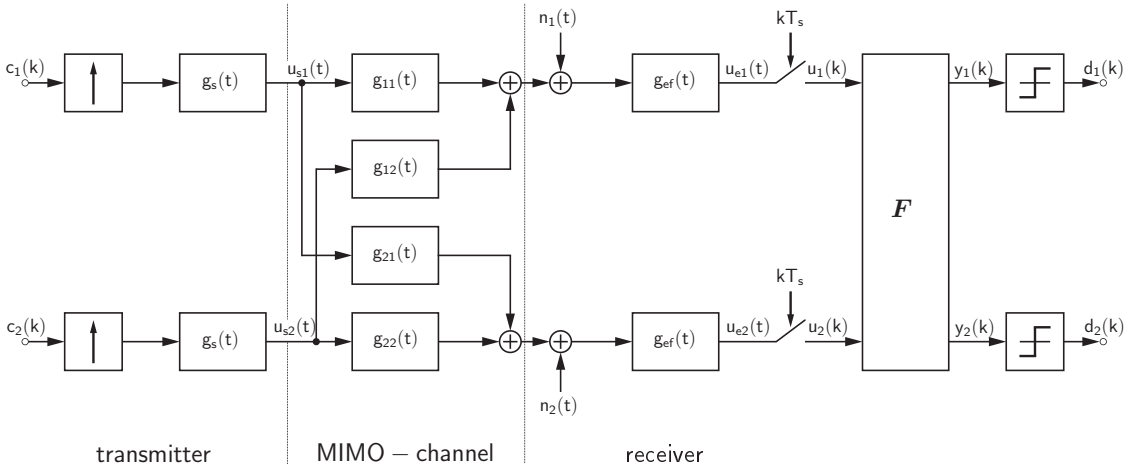

Figure 11: (2×2) MIMO baseband transmission system model with discrete zero–forcing equaliser.

system can be simplified by introducing the cumulative channel impulse response $h_{i,j}(t)$ and the filtered noise $w_i(t)$ expressed as follows

$$h_{i,j}(t) = g_\mathrm{s}(t) * g_{i,j}(t) * g_\mathrm{ef}(t), \qquad h_{i,j}(k) = h_{i,j}(t)\Big|_{kT_\mathrm{s}} \tag{18}$$

$$w_i(t) = n_i(t) * g_\mathrm{ef}(t), \qquad w_i(k) = w_i(t)\Big|_{kT_\mathrm{s}} \tag{19}$$

By utilising a data block transmission model [14, 15] a vectorial notation can be applied as follows

$$\begin{aligned} \boldsymbol{c} &= \begin{pmatrix} c[1] & c[2] & \cdots & c[K] \end{pmatrix}^\mathrm{T} \\ \boldsymbol{h}_{i,j} &= \begin{pmatrix} h_{i,j}[1] & h_{i,j}[2] & \cdots & h_{i,j}[L] \end{pmatrix}^\mathrm{T} \quad . \end{aligned} \tag{20}$$

Using the convolution matrices $\boldsymbol{H}_{i,j}$ the transmission model can be described as

$$\begin{aligned} \boldsymbol{u}_1 &= \boldsymbol{H}_{11} \cdot \boldsymbol{c}_1 + \boldsymbol{H}_{12} \cdot \boldsymbol{c}_2 + \boldsymbol{w}_1 \\ \boldsymbol{u}_2 &= \boldsymbol{H}_{21} \cdot \boldsymbol{c}_1 + \boldsymbol{H}_{22} \cdot \boldsymbol{c}_2 + \boldsymbol{w}_2 \quad . \end{aligned} \tag{21}$$

Written in matrix notation

$$\begin{pmatrix} \boldsymbol{u}_1 \\ \boldsymbol{u}_2 \end{pmatrix} = \begin{pmatrix} \boldsymbol{H}_{11} & \boldsymbol{H}_{12} \\ \boldsymbol{H}_{21} & \boldsymbol{H}_{22} \end{pmatrix} \cdot \begin{pmatrix} \boldsymbol{c}_1 \\ \boldsymbol{c}_2 \end{pmatrix} + \begin{pmatrix} \boldsymbol{w}_1 \\ \boldsymbol{w}_2 \end{pmatrix} \quad . \tag{22}$$

Simplifying this equation results in

$$\boldsymbol{u} = \boldsymbol{H} \cdot \boldsymbol{c} + \boldsymbol{w} \quad , \tag{23}$$

where the channel matrix $\boldsymbol{H}$ contains the ISI as well as the crosstalk information. For obtaining the transmitted symbols unaffected from the channel

$$\boldsymbol{F} \cdot \boldsymbol{H} = \boldsymbol{I} \tag{24}$$

has to be fulfilled, where $\boldsymbol{I}$ is a identity matrix and thus the equaliser matrix $\boldsymbol{F}$ can be obtained as follows

$$\boldsymbol{F} = (\boldsymbol{H}^{\mathrm{H}}\, \boldsymbol{H})^{-1} \boldsymbol{H}^{\mathrm{H}} \quad . \tag{25}$$

Hereinafter, the equaliser matrix $\boldsymbol{F}$ is applied to the received data vector $\boldsymbol{u}$

$$\begin{aligned} \boldsymbol{y} &= \boldsymbol{F} \cdot \boldsymbol{u} \\ \boldsymbol{y} &= \boldsymbol{c} + \boldsymbol{F} \cdot \boldsymbol{w} \quad . \end{aligned} \tag{26}$$

The benefit of applying this zero–forcing (ZF) equaliser is the orthogonalisation of the transmission channels. Thus, the resulting equalised MIMO system can be described by two independent SISO channels. The disadvantage of using the ZF equaliser is the weighting of the noise term.

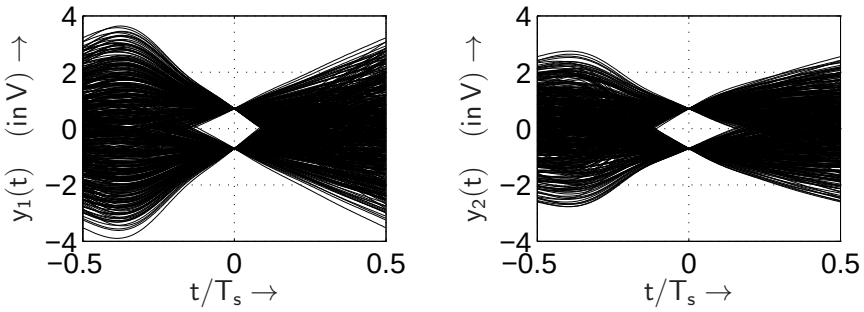

Figure 12: Eye diagram patterns of both received signals when applying zero–forcing equalisation.

Eye diagrams of both received signals in the MIMO system after equalisation are shown in Fig. 12. Using the ZF equaliser both eyes are fully opened confirming its functionality. The MIMO bit-error rate (BER) simulation results are depicted in Fig. 13 and underline the functionality of the equaliser.

5 Conclusion

In this contribution a (2×2) optical MIMO communication system, consisting of a 1.4 km multi-mode fibre and optical couplers attached to both ends, has been analysed. The estimations of the MIMO specific impulse responses have been obtained for operating wavelengths of 1576 nm and 1326 nm using optimized signal deconvolution by applying the parametric regularisation filter. It has been shown that the quality of the estimated impulse responses significantly improves and is comparable to Wiener filtering. These estimated impulse responses have been used for modelling a baseband MIMO data transmission system. In order to receive the transmitted data unaffected from the data send

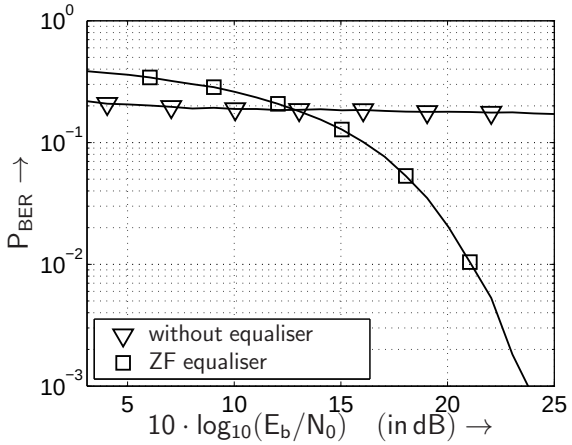

Figure 13: (2×2) MIMO BER probability as a function of bit energy E_b to noise PSD with and without applying the zero–forcing equalising method using the deconvolved MIMO impulse responses at 1576 nm operating wavelength and transmitting with a bit rate of 1.24 Gb/s.

on the neighbouring channel zero–forcing equalisation has been investigated. The successful implementation has been shown by the bit-error curves as well as by the open eye-diagram.

References

[1] A. C. Singer, N. R. Shanbhag, and Hyeon-Min Bae. Electronic Dispersion Compensation – An Overwiew of Optical Communications Systems. *IEEE Signal Processing Magazine*, 25(6):110–130, 2008.

[2] P. J. Winzer. Optical Networking beyond WDM. *IEEE Photonics Journal*, 4:647–651, 2012.

[3] D. J. Richardson, J.M. Fini, and L.E. Nelson. Space Division Multiplexing in Optical Fibres. *Nature Photonics*, 7:354–362, 2013.

[4] V. Kühn. *Wireless Communications over MIMO Channels – Applications to CDMA and Multiple Antenna Systems.* Wiley, Chichester, 2006.

[5] D. Tse and P. Viswanath. *Fundamentals of Wireless Communication.* Cambridge, New York, 2005.

[6] W. L. Gans. Calibration and Error Analysis of a Picosecond Pulse Waveform Measurement System at NBS. *Proceedings of the IEEE*, 74(1):86–90, January 1986.

[7] H. Köhnke, R. Schwinkendorf, S. Daase, A. Ahrens, and S. Lochmann. Receiver Design for an Optical MIMO Testbed. In *International Conference on Optical Communication Systems (OPTICS)*, pages 31–36, Vienna (Austria), 28.–30. August 2014.

[8] A. Ahrens and S. Lochmann. Optical Couplers in Multimode MIMO Transmission Systems: Measurement Results and Performance Analysis. In *International Conference on Optical Communication Systems (OPTICS)*, pages 398–403, Reykjavik (Iceland), 29.–31. July 2013.

[9] A. Sandmann, A. Ahrens, and S. Lochmann. Experimental Description of Multimode MIMO Channels utilizing Optical Couplers. In *15. ITG-Fachtagung Photonische Netze – ITG-Fachbericht Band 248*, pages 125–130, Leipzig (Germany), 05.–06. May 2014.

[10] A. Ahrens, A. Schröder, and S. Lochmann. Dispersion Analysis within a Measured 1,4 km MIMO Multimode Channel. In *International Conference on Optical Communication Systems (OPTICS)*, pages 391–397, Reykjavik (Island), 29.–31. July 2013.

[11] Saeed Vaseghi. *Advanced Digital Signal Processing and Noise Reduction, Second Edition*. John Wiley & Sons Ltd, Chichester, 2000.

[12] N. S. Nahman and M. E. Guillaume. *Deconvolution of Time Domain Waveforms in the Presence of Noise*. National Bureau of Standards Technical Note 1047, Boulder, Colorado 80303, October 1981.

[13] A. Sandmann, A. Ahrens, and S. Lochmann. Signal Deconvolution of Measured Optical MIMO-Channels. In *XV International PhD Workshop OWD 2013*, pages 278–283, Wisła, Poland, 19.–22. October 2013.

[14] G. G. Raleigh and John M. Cioffi. Spatio-Temporal Coding for Wireless Communication. *IEEE Transactions on Communications*, 46(3):357–366, March 1998.

[15] G. G. Raleigh and V. K. Jones. Multivariate Modulation and Coding for Wireless Communication. *IEEE Journal on Selected Areas in Communications*, 17(5):851–866, May 1999.